



ORIGINAL ARTICLE

Adsorption of cationic methylene blue dye using microwave-assisted activated carbon derived from acacia wood: Optimization and batch studies



Mohamad Firdaus Mohamad Yusop^a, Mohd Azmier Ahmad^{a,*}, Nur Ayshah Rosli^a, Mohd Edeerozey Abd Manaf^b

^a School of Chemical Engineering, Engineering Campus, Universiti Sains Malaysia, 14300 Nibong Tebal, Penang, Malaysia

^b Smart Materials Research Group, Centre of Smart System and Innovative Design (CoSSID), Faculty of Manufacturing Engineering, Universiti Teknikal Malaysia Melaka, Hang Tuah Jaya, 76100 Durian Tunggal, Melaka, Malaysia

Received 12 January 2021; accepted 9 March 2021

Available online 24 March 2021

KEYWORDS

Activated carbon;
Physicochemical activation;
Microwave heating;
Optimization;
Methylene blue;
Acacia wood

Abstract This study assesses the performance of optimized acacia wood-based activated carbon (AWAC) as an adsorbent for methylene blue (MB) dye removal in aqueous solution. AWAC was prepared via a physicochemical activation process that consists of potassium hydroxide (KOH) treatment, followed by carbon dioxide (CO₂) gasification under microwave heating. By using response surface methodology (RSM), the optimum preparation conditions of radiation power, radiation time, and KOH-impregnation ratio (IR) were determined to be 360 W, 4.50 min, and 0.90 g/g respectively, which resulted in 81.20 mg/g of MB dye removal and 27.96% of AWAC's yield. Radiation power and IR had a major effect on MB dye removal while radiation power and radiation time caused the greatest impact on AWAC's yield. BET surface area, mesopore surface area, and pore volume of optimized AWAC were found to be 1045.56 m²/g, 689.77 m²/g, and 0.54 cm³/g, respectively. Adsorption of MB onto AWAC followed Langmuir and pseudo-second order for isotherm and kinetic studies respectively, with a Langmuir monolayer adsorption capacity of 338.29 mg/g. Mechanism studies revealed that the adsorption process was controlled by film diffusion mechanism and indicated to be thermodynamically exothermic in nature.

© 2021 The Author(s). Published by Elsevier B.V. on behalf of King Saud University. This is an open access article under the CC BY license (<http://creativecommons.org/licenses/by/4.0/>).

* Corresponding author.

E-mail address: chazmier@usm.my (M.A. Ahmad).

Peer review under responsibility of King Saud University.



1. Introduction

Dyes are heavily utilized in a wide range of industries including textiles, paper, magazines, food, cosmetics, and leather (Mahapatra et al., 2021). The yearly production of synthetic dyes is between 700,000 and 1,000,000 tons worldwide and according to Daoud et al. (2017), as many as 10,000 different

types of dyes were reported in the literature. In terms of molecular structure, most synthetic dyes contain complex aromatic structure which explains their stability against light, heat, and oxidizing chemicals (Kono, 2015). Due to the molecular complexity, escaped dyes can exist in open water for a very long time and potentially harming the aquatic organisms by preventing sunlight from reaching aquatic plants (Dai et al., 2019). A highly demanded dye in textile industries with such molecular structure / complexity is methylene blue (MB) dye. This dye belongs in the basic group and upon dissociation in water, it produces positive ions. These positive ions are attracted to the negative polar region of water molecules, making MB dye to be harder to be removed in a solution. Serious health issues such as cyanosis, jaundice, tissue necrosis, methemoglobinemia, and quadriplegia have been reported when humans are exposed to MB dye for adequate time (Kushwaha et al., 2014). Porhemmat et al. (2017) stated that the degradation of MB dye products is potentially carcinogenic and mutagenic. Furthermore, the growth of plants can also be disrupted when MB dye merges with phosphate and lipid molecules in plants' cell membrane (Zhang et al., 2016).

There are many methods to treat dyes wastewater but, according to Khanday et al. (2017a, 2017b), methods like oxidation, catalytic degradation and biodegradation are not preferred due to limited efficiency, time consuming and costly. The adsorption process using activated carbon (AC) was found to be effective in treating dyes wastewater. In the study conducted by Marrakchi et al. (2016), AC was proven to be versatile due to its ability to adsorb both basic and reactive dyes. Unfortunately, commercial AC derived from lignite, bituminous coal, and petroleum coke are generally expensive and non-renewable. Besides that, AC production from coal is a highly energy demand process (Marrakchi et al., 2017). Because of that, many researchers had chosen agricultural wastes as the precursors to be converted into AC since they are cheap and available in large quantities. Some examples of these agricultural wastes are *Glyricidia sepium* (Ahmad et al., 2020), durian peel (Yusop et al., 2021), spent tea leaves (Guclu et al., 2021), date palm fiber (Melliti et al., 2021), mangosteen peel (Zhang et al., 2021), corncob (Medhat et al., 2021), *Pentace* sawdust (Khasri et al., 2018) and oil palm ash (Khanday et al., 2017a, 2017b). Apart from the cost, the operation complexity, technical flexibility, and low waste generation is among the consideration to choose the adsorption process for treating dyes in wastewater (Al-Ghouti & Al-Absi, 2020).

Generally, there are two major steps in producing AC. The first step is the carbonization process, a thermal degradation process that occurs in an absence of oxygen (Lam et al., 2016). During this step, the precursor is converted into char by subjecting it to a moderately high temperature between 400 and 600 °C. The main objective of carbonization is to increase carbon content and to build the preliminary pores network (Chen et al., 2018). The next step is the activation process which can be performed in several ways of physical activation, chemical activation, and physicochemical activation. Physical activation is conducted under an oxidizing gas environment like water steam, O₂ or CO₂ at higher activation temperature between 800 and 1100 °C, whereas chemical activation is done by impregnating the char with chemical activating agents like KOH, phosphoric acid (H₃PO₄) and zinc chloride (ZnCl₂)

before being heated once again at moderate temperature (González-García, 2018). On the other hand, physicochemical activation combines both physical and chemical activation. It starts with the impregnation of char with a chemical activating agent, followed by gasification treatment by oxidizing gas at moderately high temperature.

Process activation using a conventional furnace has some disadvantages such as high energy consumption and long activation time. Alternatively, researchers are now keener in using microwave heating techniques as the activation process (Sousa et al., 2021; Li et al., 2021; Zhou et al., 2021). According to Njoku et al. (2014), microwave energy induces the dipole rotation in the atomic scale of the material at the rate of over a million times per minute. This resulting frictional force between atoms and molecules within the material and creating heat that is distributed rapidly throughout the material (Lam et al., 2016). Because of the shorter activation time needed to activate the sample, the amount of activating gas used can be reduced as well.

Optimization in AC production is important because it can improve efficiency without adding more cost. RSM is widely employed as an optimization tool due to several advantages that it poses such as a minimum number of experiments required, the interactive effect between variables is considered, and the development of mathematical equation that relates responses with variables (Das and Mishra, 2017). Besides that, the variation in parameters can be studied with the aid of three-dimensional graphs (Ghaedi et al., 2016). In this present work, Acacia wood (AW) chip from the *Acacia mangium* species, which is a by-product in furniture industry was collected and used as a precursor to be converted into AC. In the literature, several studies utilizing acacia wood as an adsorbent to adsorb caffeine (Danish et al., 2020), chromium (VI) (Danish et al., 2012) and rhodamine B and MB dyes (Danish et al., 2018) had been done. However, these studies were using conventional furnace to activate the sample. Therefore, this study is the first to investigate the adsorption performance of MB dye using acacia wood based activated carbon derived via microwave irradiation technique.

2. Materials and methods

2.1. Materials

The adsorbate of methylene blue, MB (C₁₆H₁₈ClN₃S) dye was provided by Sigma-Aldrich (M) Sdn. Bhd., Malaysia. The chemical activating agent, KOH used during the chemical activation step was supplied by Riedel-el Haen, Germany. Gases used during carbonization and activation steps were nitrogen gas, N₂, and CO₂ which were supplied by MOX Gases Berhad, Malaysia. AW chip in the size between 5 and 10 mm was collected from furniture factory in Sungai Petani, Kedah, Malaysia.

2.1.1. Preparation of AWAC

Once collected, AW chip was washed thoroughly and then dried in oven for 72 h. 50 g of dried AW chip was loaded inside vertical tubular furnace for carbonization process to take place. The precursor was heated at 550 °C for 1 h with N₂ gas purging through the furnace at the rate of 150 cm³/min.

The resulted char was then impregnated with KOH at various impregnation ratio (IR) (0.00, 0.50, 1.25, 2.00 and 2.51 g/g), calculated as follows:

$$IR = \frac{W_{KOH}}{W_{char}} \quad (1)$$

where W_{KOH} is the weight of KOH pellet and W_{CHAR} is the weight of the char. 250 mL of deionized water was added to dissolve the KOH pellet. The impregnated sample was left in an oven for 24 h at 110 °C for chemical activation and dehydration process to occur. The thermal step is introduced to further removing moisture with the assistance of acid. During this step, reactions of depolymerization, dehydration, and condensation take place, which causing higher carbon yields with less tar formations and volatiles (Bedia et al., 2020). The depolymerization of cellulose, hemicellulose, and lignin which catalysed by KOH has led to decrease in mechanical resistance, has subsequently causes swelling of the particle. The condensation reaction may induce the formation of cross-linking and formation of small pores (Izgi et al., 2019). After that, the sample was heated in an improvised microwave oven (EMM2001W, Sweden) at different radiation power (144, 264, 440, 616 and 736 Watt) and different radiation time (2.60, 4.00, 6.00, 8.00 and 9.40 min). The CO₂ gas was purged through the microwave oven at the rate of 150 cm³/min to provide gasification effect to the sample. Sample that was retrieved from microwave oven was washed with hot deionized water and 0.1 M HCl solution until the pH of the washing solution was in the range between 6.5 and 7. Lastly, the sample was kept in oven for 24 h at 110 °C to dry. Once dried, the yield of AWAC was determined by using the following equation:

$$Yield = \frac{W_f}{W_i} \times 100\% \quad (2)$$

where W_f and W_i are dried weight of AWAC and dried weight of precursor, respectively.

2.1.2. Characterization methods

Characterization of AWAC was done by nitrogen adsorption-desorption measurements to determine the Brunauer-Emmet-Teller (BET) surface area, Barrett-Joyner-Halenda (BJH) pore size distribution (PSD), total pore volume and average pore diameter of the sample using Micromeritics volumetric adsorption analyser (ASAP 2010), proximate analysis by using simultaneous thermal analyzer (Perkin Elmer STA 6000, USA), elemental analysis by using elemental analyzer (Perkin Elmer Series II 2400, USA), surface morphology using scanning electron microscopy (SEM) (LEO SUPRA 55VP, Germany), surface chemistry using Fourier transforms infrared spectroscopy (FTIR) (Shidmazu Prestige 21, Japan) and zeta potential using zeta potential analyzer (Zetasizer Nano Series DKSH).

2.2. Experimental design

The objective of this study was to find the optimum preparation conditions of AWAC by employing a standard RSM design known as Central Composite Design (CCD). In this study, Design Expert software (STAT-EASE Inc. Minneapolis, USA) version 6.0.6 was used to analyse the experimental data. The variables were set to be radiation power

(X_1), radiation time (X_2) and IR (X_3) while the responses were MB removal (Y_1) and AWAC's yield (Y_2). Table 1 summarizes the variables, responses and variables' experimental range and levels. Since 3 variables were studied, a design matrix with 20 experiments were generated by CCD which comprised of 8 factorial points, 6 axial points and 6 replicates. The replication is used to determine the error of experiments. The corresponding model is a quadratic model, expressed by the following equation:

$$Y = (b_0 + \varepsilon) + \sum_{i=1}^3 b_i x_i + \sum_{i=1}^3 b_{ii} x_i^2 + \sum_{i=1}^3 \sum_{j=i+1}^3 b_{ij} x_i x_j + e_i \quad (3)$$

where Y is the predicted response, b_0 , b_i , b_{ij} and b_{ii} are the constant coefficient, linear coefficient, interaction coefficient and quadratic coefficient, respectively, x_i and x_j are the coded values of the AWAC preparation variables and e_i is the error. The adsorption process was performed using 250 mL of conical flask with MB initial concentration of 100 mg/L, solution volume of 200 mL and AWAC dosage of 0.2 g. The conical flask was loaded inside water bath shaker and the shaker speed was set at 150 rpm and temperature of 30 °C. The pH of the solution was kept original without any alterations.

2.3. Equilibrium study

The equilibrium study was performed to study the effect of different initial concentration, effect of solution temperature and effect of solution pH on MB dye adsorption. To study the effect of initial concentration, six different initial concentration of 25, 50, 100, 200, 250 and 300 mg/L were prepared. 200 mL of each of these solutions were filled inside 250 mL of Erlenmeyer flasks. 0.2 g of AWAC was added in each flask and these flasks were loaded in a water bath shaker for 24 h. The agitation speed was set at 150 rpm, temperature was set at 30 °C and pH was kept original.

To study the effect of solution temperature, three different temperature of 30, 45 and 60 °C were used while pH was kept original. To study the effect of solution pH, six different pH of 2, 4, 6, 8, 10 and 12 was used while the temperature was fixed constant at 30 °C. The pH of MB solution was altered using sodium hydroxide (NaOH) and hydrochloric acid (HCl). For both temperature and pH studies, fixed initial concentration of 300 mg/L and AWAC dosage of 0.2 g per 200 mL of MB solution were chosen. All experiments were repeated three times and average data was used. The concentration of MB dye solution was measured at 668 nm by using UV-vis spectrophotometry (Agilent Cary 60, USA). For equilibrium studies, the amount of MB dye adsorbed by AWAC and MB dye removal percentage were given by Eq. (4) and Eq. (5), respectively, as follows:

$$q_e = \frac{(C_o - C_e)V}{W} \quad (4)$$

$$\% \text{ Removal} = \frac{C_o - C_e}{C_o} \times 100\% \quad (5)$$

where C_o and C_e are the concentration of MB dye initially and at equilibrium, respectively; V is the volume of solution (L), and W is the weight of AWAC used (g).

Table 1 Experimental variables and levels.

		Unit	Notation	Coded values				
				-1.682	-1	0	+1	+1.682
Variables	Radiation power	Watt (W)	X ₁	144.00	264.00	440.00	616.00	736.00
	Radiation time	Minutes (min)	X ₂	2.60	4.00	6.00	8.00	9.40
	IR	g/g	X ₃	0.00	0.50	1.25	2.00	2.51
Responses	MB dye removal	mg/g	Y ₁	-	-	-	-	-
	AWAC's yield	%	Y ₂	-	-	-	-	-

The equilibrium data was tested using four isotherm models namely Langmuir, Freundlich, Temkin and Dubinin-Radushkevich. Their equations are given as follows:

Langmuir (Langmuir, 1918):

$$q_e = \frac{Q_m K_L C_e}{1 + K_L C_e} \quad (6)$$

Freundlich (Freundlich, 1906):

$$q_e = K_F C_e^{1/n_F} \quad (7)$$

Temkin (Temkin and Pyzhev, 1940):

$$q_e = \frac{RT}{B} \ln(AC_e) \quad (8)$$

Dubinin-Radushkevich (Redlich and Peterson, 1959):

$$q_e = q_{DR} \exp \left[\frac{(RT \ln(1 + 1/C_e))^2}{-2\epsilon^2} \right] \quad (9)$$

where Q_m is maximum adsorption capacity; K_L is the constant of Langmuir; K_F and n_F are constants of Freundlich; B and A are constants of Temkin, q_{DR} is the adsorption capacity, R is the universal gas constant, T is temperature and ϵ is free energy. These non-linear equations were solved using Microsoft Excel Solver version 2016.

2.4. Kinetic study

The similar procedure in equilibrium study was carried out in kinetic study using MB solution with six different initial concentration of 25, 50, 100, 200, 250 and 300 mg/L. The desired contact time is ranging from 15 to 180 min. AWAC dosage, solution volume, solution temperature and agitation speed were set to be 0.2 g, 200 mL, 30 °C and 150 rpm, respectively. No alteration in pH solution is done in kinetic study. The data of adsorption kinetic were fitted on five kinetic models namely pseudo-first order, pseudo-second order, Elovich, Intraparticle diffusion and Boyd plot. Their equations are given as follows:

Pseudo-first order (PFO) (Lagergren and Svenska, 1898):

$$q_t = q_e [1 - \exp(-k_1 t)] \quad (10)$$

Pseudo-second order (PSO) (Ho and McKay, 1999)

$$q_t = \frac{k_2 q_e^2 t}{1 + k_2 q_e t} \quad (11)$$

Elovich (Aeenjan and Javanbakht, 2018):

$$q_t = \frac{1}{\beta} \ln(x\beta) + \frac{1}{\beta} \ln t \quad (12)$$

Intraparticle diffusion (Boopathy et al., 2013):

$$q_t = k_{t,i} t^{\frac{1}{2}} \quad (13)$$

Boyd plot (Islam et al., 2017):

$$B_t = -0.4977 - \ln \left(1 - \frac{q_t}{q_e} \right) \quad (14)$$

where k_1 is rate constant for PFO, k_2 is rate constant for PSO, α is sorption constant of adsorbate, β is constant of desorption, $k_{t,i}$ is rate constant for intraparticle diffusion. The error percentage was calculated to find the percentage of deviation between calculated q_e , $q_{e,cal}$ and experimental q_e , $q_{e,exp}$ using the following equation:

$$Error (\%) = \left| \frac{q_{e,exp} - q_{e,cal}}{q_{e,exp}} \right| \times 100\% \quad (15)$$

2.5. Thermodynamic study

The parameters obtained from thermodynamics study are important in predicting the adsorption behaviour under the influence of temperature. The Van't Hoff equation was used to calculate ΔH° and ΔS° :

$$\ln K_c = \frac{\Delta S^\circ}{R} - \frac{\Delta H^\circ}{RT} \quad (16)$$

Gibbs free energy, ΔG° was determined by using the following equation:

$$\Delta G^\circ = -RT \ln K_c \quad (17)$$

The Arrhenius equation was used to determine activation energy as follows:

$$\ln k_2 = \ln A - \frac{E_a}{RT} \quad (18)$$

where ΔH° is the enthalpy change (kJ mol^{-1}), ΔS° is the entropy change ($\text{kJ mol}^{-1} \text{K}^{-1}$), ΔG° is the Gibbs free energy (kJ mol^{-1}), K_c is the equilibrium constant (dimensionless), R is the universal gas constant ($8.314 \text{ J mol}^{-1} \text{K}^{-1}$), T is absolute temperature, k_2 is rate constant of PSO and A is Arrhenius factor. According to Lima et al. (2019), K_c can be calculated by using the following equation:

$$K_c = \frac{1000 \frac{\text{mg}}{\text{g}} \times K_L \times \text{molecular weight of adsorbate} \times [\text{adsorbate}]^\circ}{\gamma} \quad (19)$$

where $[\text{adsorbate}]^\circ$ and γ are the standard concentration of the adsorbate, which concentration by definition is 1 mol/L at standard conditions and coefficient of activity of the adsorbate (dimensionless), respectively.

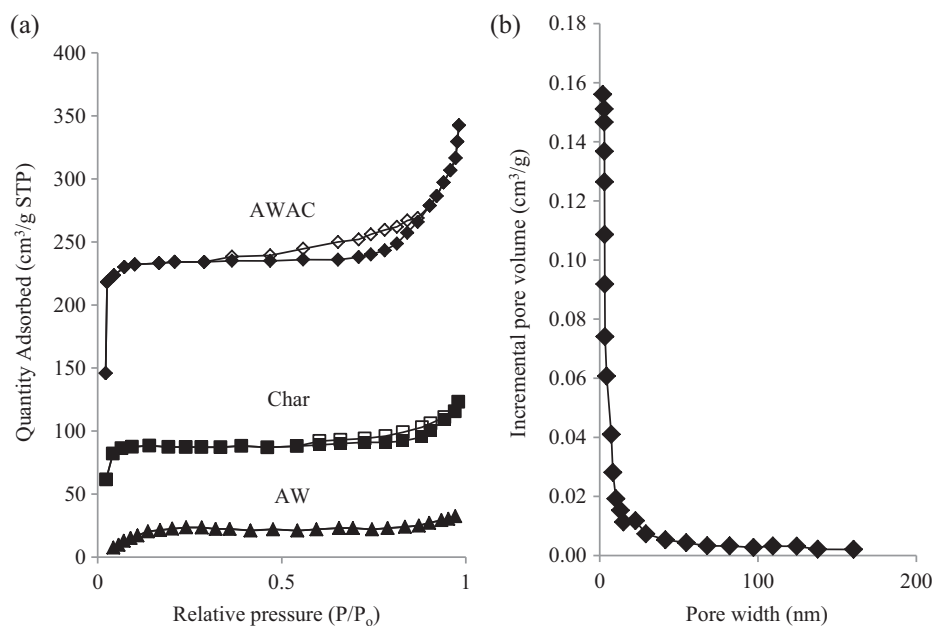


Fig. 1 (a) N_2 adsorption–desorption isotherms of samples and (b) PSD of AWAC.

3. Results and discussions

3.1. Characterization of samples

The N_2 adsorption–desorption isotherm for optimized AWAC, char and AW are given in Fig. 1(a). AW manifested a Type II isotherm whereas both AW char and AWAC demonstrated combination of Type I and Type II sorption isotherms, which indicates the existence of micropores and mesopores. Fig. 1(b) shows the pore size distribution (PSD) for AWAC. It was found that the pore size of AWAC was accumulated in the range of 1.64–1.91 nm similar to the trends found by Ahmad, et al. (2020) and Jang and Kan (2019) in their characterization study of AC. MB has a molecular size of 1.382 nm in length and 0.92 nm in width (Jia et al., 2018), therefore it is enables to agglomerate on the surface of AWAC with average pore diameter of 2.78 nm.

The BET surface area for precursor was found to be $1.12 \text{ m}^2/\text{g}$ and after carbonization process took place, this value increased to $425.41 \text{ m}^2/\text{g}$ in char. This was caused by the removal of moisture content and light volatile matter compound from precursor. Once these substances leave precursor, vacant spaces which associated with pores network was formed. Upon chemical activation, metallic potassium ions, K^+ travelled deep into these pores network and increased them. After that, the following gasification treatment causing CO_2 molecules to bombard the surface and the internal side of impregnated char, causing the pores development process

to be further enhanced. Microwave energy was responsible in heating the char and causing removal of heavy volatile matter. This resulted in an increment of BET surface area to become $1045.56 \text{ m}^2/\text{g}$ in AWAC. Physicochemical activation also succeeded in increasing the mesopores surface area from $268.40 \text{ m}^2/\text{g}$ in char to $689.77 \text{ m}^2/\text{g}$ in AWAC. The total pore volume for AWAC was $0.5350 \text{ cm}^3/\text{g}$ whereas the average pore diameter for AWAC was 2.78 nm, which lies in the mesopores region.

The proximate and elemental analyses of precursor and AWAC are given in Table 2. The fixed carbon for precursor was found to be relatively high of 24.75%, thus making it a suitable choice of precursor in the first place. Based on proximate analysis, the composition of precursor was dominated by moisture of 12.55% and volatile matter of 57.20%. However, these components were successfully removed during carbonization and physicochemical activation, thus their values significantly dropped in AWAC to be 5.23% and 10.74% for moisture and volatile matter, respectively. On contrary, percentage of fixed carbon in AWAC rose sharply to 81.14%. Low ash content of 2.89% in AWAC was a manifestation that the heat treatment used during carbonization and microwave heating were at the right range and no combustion occur in both processes. In elemental analysis, the C element increased tremendously from 20.92% in precursor to 78.60% in AWAC. On the other hand, other elements of H, S, N and O were decreased after carbonization and physicochemical activation took place.

Table 2 Proximate and elemental analyses of the samples.

	Proximate analysis (%)				Elemental analysis (%)			
	Moisture	Volatile matter	Fixed carbon	Ash	C	H	S	(N + O)
Precursor	12.55	57.20	24.75	5.50	20.92	9.89	0.09	69.10
AWAC	5.23	10.74	81.14	2.89	78.60	7.20	0.01	14.19

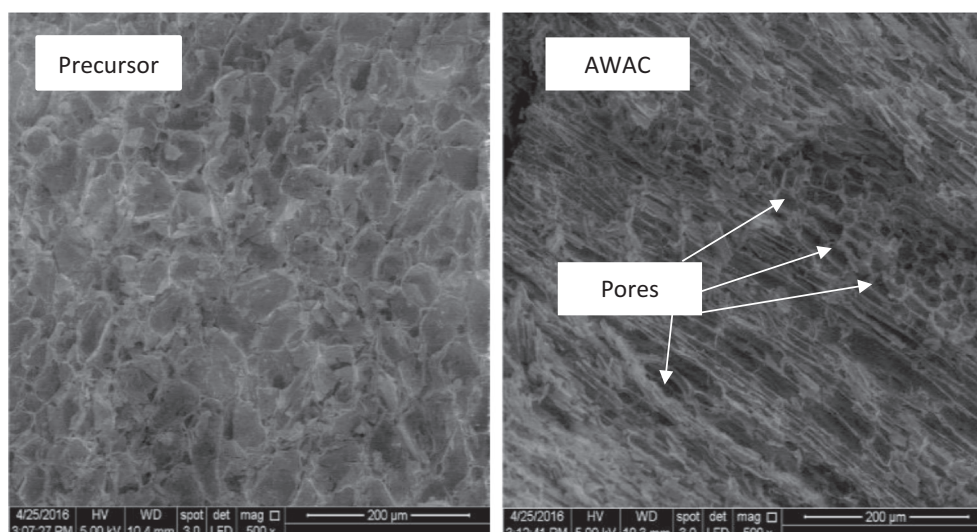


Fig. 2 SEM images of precursor and AWAC.

The SEM images of precursor and AWAC are shown in Fig. 2. These images are useful to recognize the inner carbon structure morphology (Ilnicka et al., 2020). The shape structure of precursor and AWAC was found to be different. Unlike the precursor, AWAC's structure was found to be filled with numerous cavities that exist in different sizes. These cavities are formed due to the volatilization of moisture and volatile matter that occurred during carbonization and activation process. Similar result was observed in the work done by Lopes et al. (2021) where significant changes in terms of formation of cavities on AC's surface occurred after activation process took place. Metallic potassium, K^+ from KOH was known to penetrate deep inside the surface of sample, thus

creating more cavities (Yusop et al., 2021) distributed on the whole surface of AWAC.

The FTIR spectrum for precursor and AWAC is given in Fig. 3. Peaks that exist on both precursor and AWAC were medium band $3584\text{--}3700\text{ cm}^{-1}$ that represents O-H in alcohol (Kacan, 2016), strong band $1500\text{--}1550\text{ cm}^{-1}$ that represents NO— compound, strong band $1638\text{--}1648\text{ cm}^{-1}$ that represents C=C in alkene (Zhou et al., 2017) and strong band 690 cm^{-1} that represents mono-substituted benzene (Yorgun and Yildiz, 2015). According to Arbanah et al. (2013), functional groups with negatively charge polarity like hydroxyl, O—H and nitro, NO— promote the adsorption process between cationic MB dye and AWAC. Several peaks that were unable to withstand

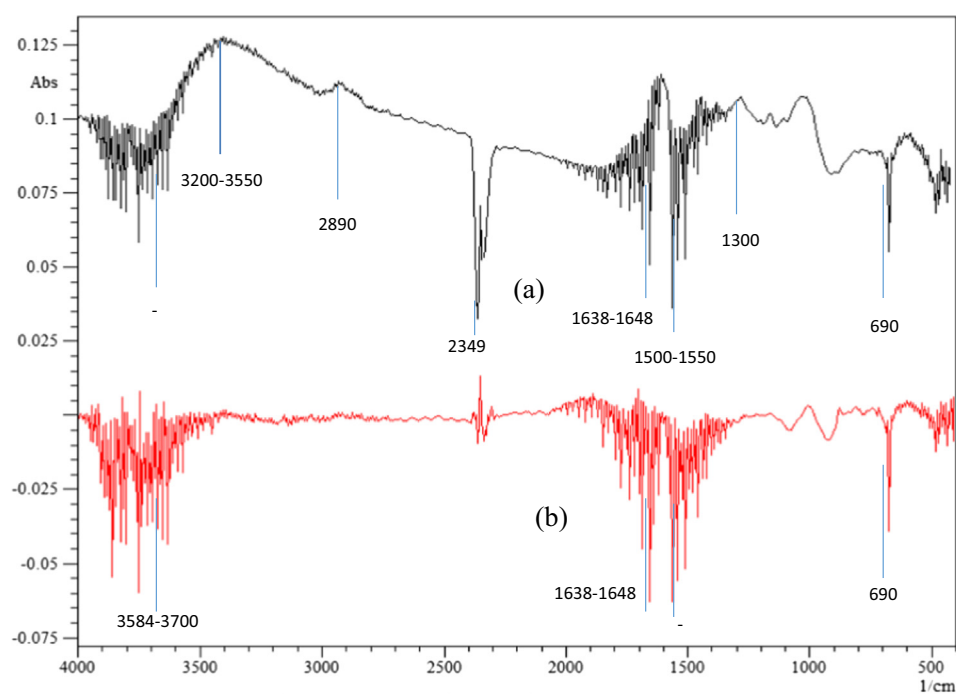


Fig. 3 FTIR spectrum for (a) precursor and (b) AWAC.

the heat treatment during carbonization and physicochemical activation steps were broad band 3200–3550 cm^{-1} that represents O–H in alcohol (Ghaedi et al., 2015), weak band 2890 cm^{-1} that represents C–H in methylene group (Kumar and Jena, 2016), strong band 2349 cm^{-1} that represents COOH in carboxyl group (Agarwal et al., 2017) and weak band 1300 cm^{-1} that represents C–O in phenol, ether or ester (Kumar and Jena, 2016). These peaks were visible in spectrum of precursor and diminished in the spectrum of AWAC.

The surface of AC carries a net charge, also known as zeta potential, which affects the degree of affinity of adsorbate towards adsorbent (Maršálek and Švidrnoch, 2020). The magnitude of zeta potential can easily be affected by the pH of environment that the surface is exposed to. Fig. 4 shows the zeta potential curve for AWAC. AWAC was found to have zeta potential value of -5.17 . This negative value indicated that the surface of AWAC provided a good attraction towards positively charged adsorbate.

3.2. Optimization studies

3.2.1. Regression model development

Table 3 depicts the complete experimental design matrix for the AWAC's preparation. For both responses of MB dye removal and AWAC's yield, the software had suggested quadratic model. The range for experimental values were 66.16 to 91.60 mg/g and 17.04 to 27.98% for MB removal and AWAC's yield, respectively. The empirical models in the form

of coded factors that relate the responses and variables were given as follows:

MB dye removal, Y_1

$$Y_1 = 91.33 + 4.21X_1 + 2.31X_2 + 3.29X_3 - 5.53X_1^2 - 3.72X_2^2 - 5.79X_3^2 - 0.83X_1X_2 - 1.02X_1X_3 - 0.61X_2X_3 \quad (20)$$

AWAC's yield, Y_2

$$Y_2 = 27.48 - 2.73X_1 - 1.63X_2 - 1.14X_3 - 1.93X_1^2 - 2.49X_2^2 - 2.92X_3^2 + 0.39X_1X_2 - 0.48X_1X_3 - 0.70X_2X_3 \quad (21)$$

The plot of predicted versus actual for MB removal and AWAC's yield are shown in Fig. 5(a) and (b), respectively. Based on these plots, four parameters were used to validate these plots which are correlation coefficient, R^2 , adjusted R^2 , standard deviation and adequate precision (AP). The quality of the model is getting better as the value of R^2 approaching 1. Adjusted R^2 is the better version of R^2 where the insignificant data were not considered in the calculation. Larger value of standard deviation indicates higher deviation of predicted data from actual data and vice versa. AP measured the adequacy of model to estimate the response and any value above 4 were desirable for it (Bashir et al., 2010). The models in Eq. (20) and Eq. (21) were good, judging from the high R^2 values of 0.9781 and 0.9777, respectively. These R^2 values reflect that

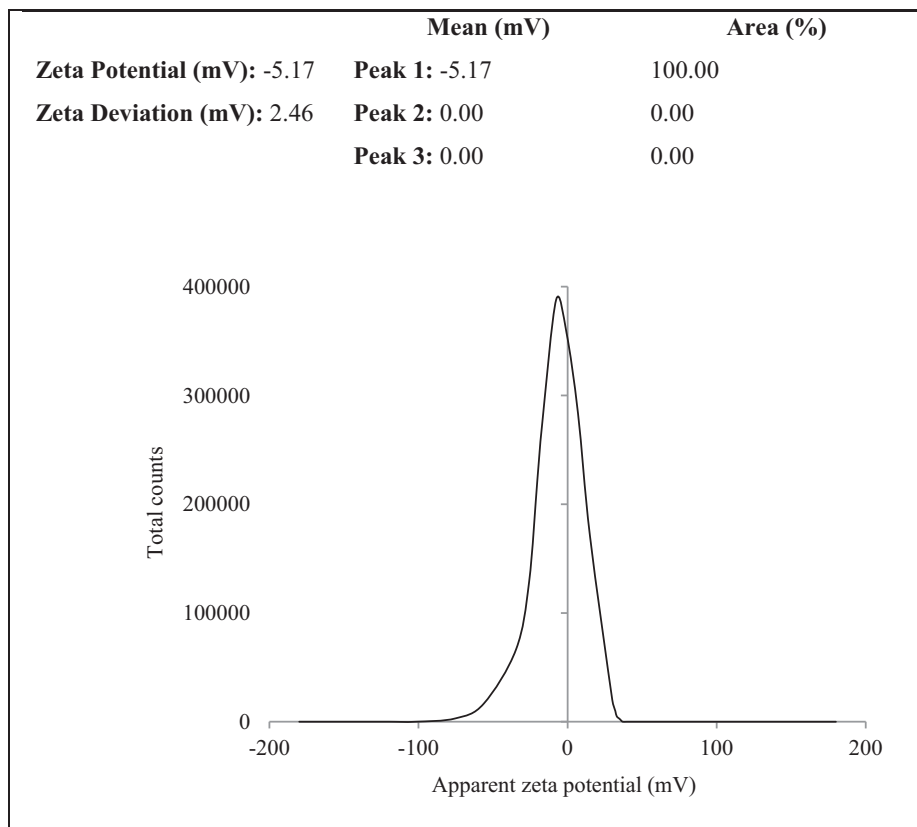
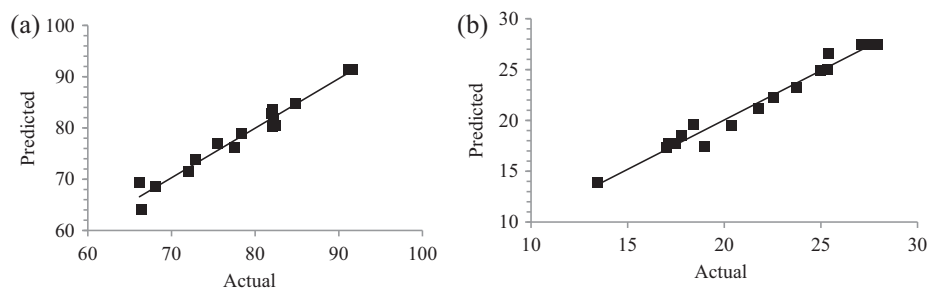


Fig. 4 Zeta potential curve of AWAC.

Table 3 Complete experimental design matrix for AWAC's preparation.

Run	AWAC's preparation variables			Responses	
	Radiation power, X_1 (watt)	Radiation time, X_2 (min)	IR, X_3	MB removal, Y_1 (mg/g)	AWAC's yield, Y_2 (%)
1	264 (-1)	4.0 (-1)	0.50 (-1)	66.38	25.00
2	440 (0)	2.6 (-1.628)	1.25 (0)	75.53	23.77
3	440 (0)	6.0 (0)	1.25 (0)	91.30	27.42
4	264 (-1)	4.0 (-1)	2.00 (+1)	72.90	25.37
5	440 (0)	6.0 (0)	1.25 (0)	91.43	27.96
6	440 (0)	6.0 (0)	1.25 (0)	91.27	27.48
7	736 (+1.628)	6.0 (0)	1.25 (0)	82.01	18.98
8	440 (0)	6.0 (0)	1.25 (0)	91.16	27.79
9	144 (-1.628)	6.0 (0)	1.25 (0)	68.10	25.41
10	264 (-1)	8.0 (+1)	2.00 (+1)	78.43	20.37
11	440 (0)	6.0 (0)	2.51 (+1.628)	82.48	17.04
12	264 (-1)	8.0 (+1)	0.50 (-1)	72.10	22.57
13	440 (0)	6.0 (0)	1.25 (0)	91.60	27.11
14	440 (0)	9.4 (+1.628)	1.25 (0)	84.83	17.48
15	616 (+1)	4.0 (-1)	0.50 (-1)	77.50	18.44
16	616 (+1)	8.0 (+1)	2.00 (+1)	82.14	13.45
17	616 (+1)	8.0 (+1)	0.50 (-1)	82.13	17.80
18	616 (+1)	4.0 (-1)	2.00 (+1)	82.17	17.10
19	440 (0)	6.0 (0)	1.25 (0)	91.41	27.06
20	440 (0)	6.0 (0)	0.00 (-1.628)	66.16	21.80

**Fig. 5** Plot of predicted versus actual for (a) MB removal and (b) AWAC's yield.

97.81% and 97.77% of total variation in MB dye removal and AWAC's yield, respectively were contributed by the variables studied. Furthermore, low standard deviation was also obtained for Eq. (20) of 1.79 and Eq. (21) of 0.94. Adjusted R^2 and AP values for Eq. (20) were 0.9583 and 21.58, respectively whereas for Eq. (21), the values were 0.9576 and 20.52, respectively. Therefore, the models developed in this study were beyond adequate to predict the responses.

Normal plot of residuals for MB removal and AWAC's yield are given in Fig. 6(a) and (b), respectively. These plots are useful to further confirm the adequacy of the developed models. Based on Fig. 6, it was found that the residuals generally fall on a straight line, thus indicating that the errors are distributed normally.

3.2.2. Analysis of variance (ANOVA)

Analysis of variance (ANOVA) is helpful in interpreting the experimental data. According to Tounsadi et al. (2016), if ANOVA produced a value for Prob > F that is less than 0.05 and high value of F value (Liew et al., 2018), it signified that the term model was significant to the response and the result was not random. The ANOVA results for MB dye removal and AWAC's yield are given in Table 4(a) and (b),

respectively. The Prob > F value for the model of both responses of MB dye removal and AWAC's yield were <0.0001 and <0.0001, respectively, thus confirming that both of these models were significant. Lack of fit was found to be insignificant to MB removal and AWAC's yield responses due to the Prob > F value of 0.0765 and 0.7120, respectively. Insignificant lack of fit verified that variables used have notable effects on the studied responses and the designed models fitted the experimental data well (Melliti et al., 2021).

Based on Table 4(a), the significant terms for MB dye removal response were radiation power (X_1), quadratic effect of radiation power (X_1^2), radiation time (X_2), quadratic effect of radiation time (X_2^2), IR (X_3) and quadratic effect of IR (X_3^2) whereas the insignificant terms were the ones not mentioned. Based on F-value, radiation power of 75.63 and IR of 46.24 were found to contribute majorly to this response while radiation time of 22.67 had relatively minor effect on this response. Based on Table 4(b), the significant terms for AWAC's yield response were radiation power (X_1), radiation time (X_2), IR (X_3), quadratic effect of radiation power (X_1^2), quadratic effect of radiation time (X_2^2) and quadratic effect of IR (X_3^2) where other terms were not mentioned are not significant to the response. Based on F-value, radiation power of

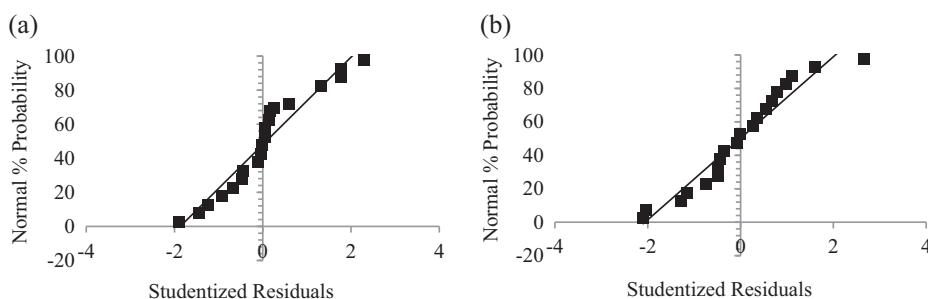


Fig. 6 Normal plot of residuals for (a) MB removal and (b) AWAC's yield.

Table 4a ANOVA result for MB dye removal.

Source	Sum of Squares	DF	Mean Square	F Value	Prob > F
Model	1428.01	9	158.67	49.53	< 0.0001
x_1	242.29	1	242.29	75.63	< 0.0001
x_2	72.61	1	72.61	22.67	0.0008
x_3	148.12	1	148.12	46.24	< 0.0001
x_1^2	441.19	1	441.19	137.72	< 0.0001
x_2^2	119.54	1	119.54	62.29	< 0.0001
x_3^2	483.60	1	483.60	150.96	< 0.0001
x_1x_2	5.53	1	5.53	1.73	0.2183
x_1x_3	8.34	1	8.34	2.60	0.1376
x_2x_3	2.94	1	2.94	0.92	0.3606
Residual	32.04	10	3.20		
Lack of fit	31.92	5	6.38	27.74	0.0765
Pure error	0.12	5	0.23		
Cor Total	1460.05	19			

Table 4b ANOVA result for AWAC's yield.

Source	Sum of Squares	DF	Mean Square	F Value	Prob > F
Model	386.94	9	42.99	48.70	< 0.0001
x_1	102.06	1	102.06	115.61	< 0.0001
x_2	36.41	1	36.41	41.24	< 0.0008
x_3	17.65	1	17.65	19.99	0.0012
x_1^2	53.91	1	53.91	61.07	< 0.0001
x_2^2	89.42	1	89.42	101.30	< 0.0001
x_3^2	122.63	1	122.63	138.91	< 0.0001
x_1x_2	1.23	1	1.23	1.40	0.2647
x_1x_3	1.86	1	1.86	2.11	0.1770
x_2x_3	3.89	1	3.89	4.41	0.0621
Residual	8.82	10	0.88		
Lack of fit	8.18	5	1.64	12.73	0.7120
Pure error	0.64	0.64	5	0.13	
Cor Total	395.47	19			

115.61 has the most significant effect to this response, followed by radiation time of 41.24. IR had the least effect to this response with F-value of 19.99.

3.2.3. Three-dimensional (3D) response surface of AWAC

The effect of the variables on the responses can be understood better by viewing the three-dimensional (3D) response surface. Fig. 7(a) and (b) show the 3D response surface plots for MB dye removal and AWAC's yield, respectively. Since ANOVA results revealed that MB removal was significantly affected by radiation power and IR whereas AWAC's yield was deeply

affected by radiation power and radiation time, therefore the 3D surface plots only showed the effect of these variables only. For MB dye removal response, radiation power and IR were varied within experimental ranges while the radiation time was fixed at zero level. For AWAC's yield response, radiation power and radiation time were varied within experimental ranges while IR was fixed at zero level.

Based on Fig. 7(a), lowest MB dye removal took place when radiation power and IR were 264 W and 0.5 g/g, respectively. When both of these variables increased, MB dye removal increased steadily as well. This can be explained by

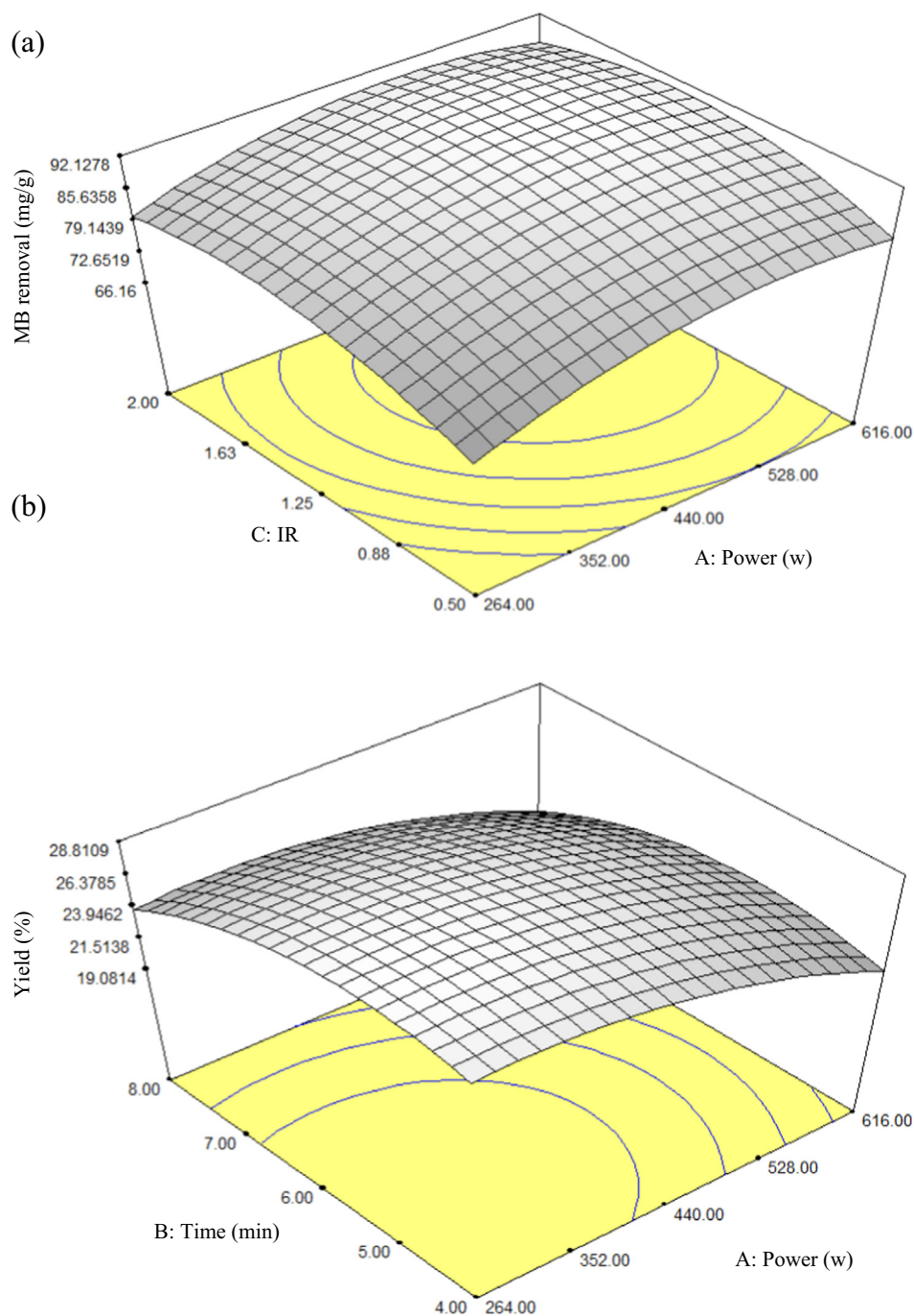


Fig. 7 3D response surface plots for (a) MB dye removal and (b) AWAC's yield.

the fact that an increased in radiation power leads to cracking reaction that improved elimination of heavy volatile matter in char, leaving more vacant sites and pores to be developed, thus increasing adsorption capacity (Wan Mahari et al., 2016). By increasing IR, more K^+ ions were available to penetrate deep into char, causing more pores to develop, thus improving adsorption capacity (Rashidi and Yusup, 2017). It was noticed that at extremely high level of radiation power, MB dye removal dropped a bit. According to Foo and Hameed (2012), excess energy can cause a small amount of carbon to burn, and rupture the existing pores, thus reducing adsorption performance of AC.

Radiation power and radiation time were found to have a negative effect on AWAC's yield as shown in Fig. 7(b). Due to this, AWAC's yield reached its maximum value when radiation power and radiation time were at their lowest level of 264 W and 4.0 min, respectively. An increased in radiation power promotes the aggressive volatilization process that leads to reduction of weight for AWAC. By increasing radiation time, it allowed this volatilization process to be elongated, thus reducing AWAC's yield even more. It was observed by Ghani et al. (2017) that a sample that was exposed to microwave heating beyond its optimum radiation time decreased in yield significantly.

Table 5 Model validation for AWAC's preparation.

Variables			Responses					
Radiation power, X_1 (watt)	Radiation time, X_2 (min)	IR, X_3 (g/g)	MB removal, Y_1 (mg/g)			AC's yield, Y_2 (%)		
			Predicted	Actual	Error	Predicted	Actual	Error
360	4.50	0.90	81.20	81.55	0.43	27.96	28.51	1.93

3.2.4. Optimization of AWAC's preparation variables

Producing AC with high adsorption performance and yield were challenging. Because of that, RSM based on CCD was employed in this study to find optimum values of variables for AWAC's preparation. The responses of MB dye removal and AWAC's yield were set to be maximum. On contrary, the variables consisted of radiation power, radiation time and IR were set to be in the range. Table 5 shows the model validation for AWAC's preparation. The optimum values for AWAC's preparation variables were found to be 360 W, 4.50 min and 0.90 g/g for radiation power, radiation time and IR, respectively. These optimum values produce AWAC with MB dye removal of 81.20 mg/g and yield of 27.96%. Small error percentage for MB dye removal of 0.43% and AWAC's yield of 1.93% indicated that the models developed in this study were excellent in predicting the responses. High desirability was obtained for this model, which is 0.986, thus signified the optimal fitting of the studied factors (Amdoun et al., 2018).

3.3. Equilibrium studies

3.3.1. Effect of contact time and initial MB dye concentration

The MB dye adsorption uptakes by AWAC at different initial concentration between 25 and 300 mg/L at 30 °C and pH 7 are

shown in Fig. 8. It can be seen that the adsorption uptakes increased from 22.96 to 210.10 mg/g as the MB dye initial concentrations increased from 25 to 300 mg/L. At higher initial concentrations, mass transfer driving force becomes higher as well. Higher driving force made it easier to overcome mass transfer resistance between MB dye in solution and solid phase, thus explaining higher MB uptakes at higher initial concentrations (Tharaneedhar et al., 2017). This finding was in agreement with the work done by Yusop et al. (2021) and Ahmad et al. (2020). MB dye solution with lower initial concentrations (25, 50 and 100 mg/L) needed shorter contact time between 4 and 6 h to reach equilibrium state. On contrary, equilibrium state was attained by higher MB dye initial concentrations (200, 250 and 300 mg/L) at higher contact time of 22 to 24 h. Equilibrium state was achieved faster at lower initial concentrations due to less competition for MB dye molecules to be adsorbed by AWAC and vice versa.

3.3.2. Effect of solution temperature and pH

MB adsorption capacity at different solution temperature is shown in Fig. 9. When the temperature of MB dye solution was increased from 30 to 60 °C, the adsorption capacity of AWAC was found to reduce from 210.21 to 179.85 mg/g. Poor adsorption performance of AWAC was contributed by the increasing solubility of MB dye molecules at higher solution

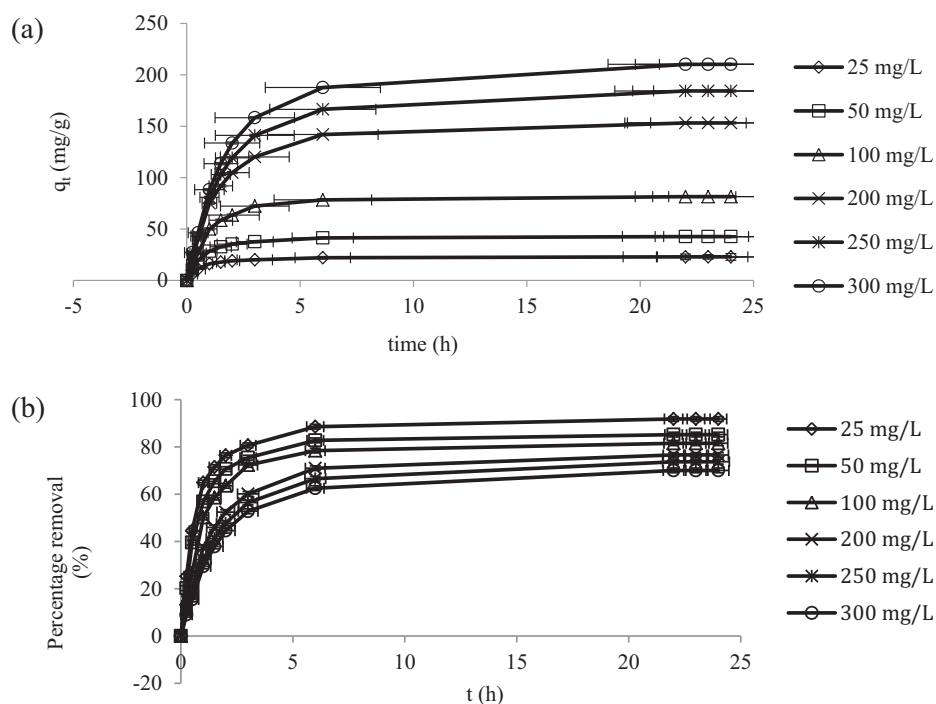


Fig. 8 (a) MB dye adsorption uptakes by AWAC and (b) MB percentage removal at different initial concentrations.

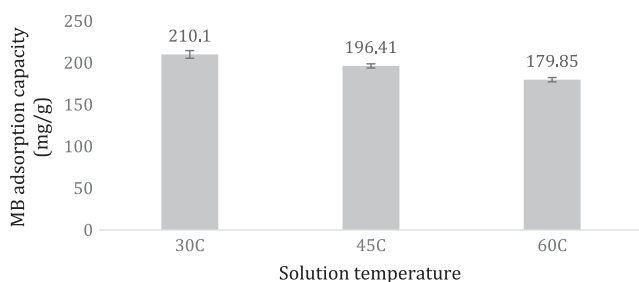


Fig. 9 MB adsorption capacity at different solution temperature.

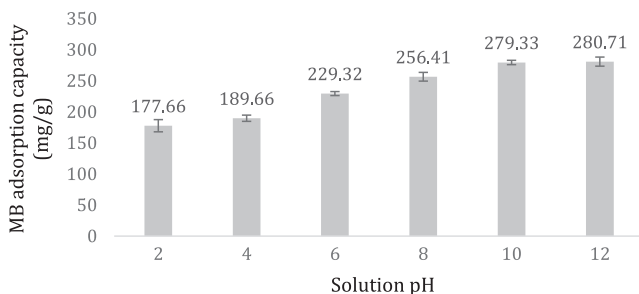


Fig. 10 MB adsorption capacity at different solution pH.

temperature. According to Abbaszadeh et al. (2016), adsorbate molecules posed higher energy at higher solution temperature, thus enabled them to escape from solid phase to bulk phase. In addition, electrostatic interaction between cationic MB dye and the negatively charged functional groups in AWAC became weaker at higher solution temperature, therefore promoting desorption process (Domic et al., 2015). In the study of MB dye removal by *Moringa oleifera* leaf-based AC, the percentage removal dropped from above 96.50% to below 95.75% when the solution temperature was raised from 21.85 °C to 51.85 °C (Do et al., 2021). Similarly, MB adsorption capacity was found to decrease from 218.48 to 197.45 mg/g as solution temperature increased from 30 °C to 60 °C in the study conducted by Ahmad et al. (2021).

The pH of dye solution can affect the adsorption performance of AC due to the existence of excess H^+ and OH^- ions in acidic and alkaline conditions, respectively (Beltrame et al., 2018). These ions can affect the zeta potential of adsorbent's

surface as well. As mentioned previously in Section 3.1, the zeta potential value for AWAC was -5.17 . This negative value signified that surface of AWAC was negatively charged in its original state. The adsorption performance at different pH is given in Fig. 10. Adsorption performance of AWAC was the worst at solution pH of 2 with MB adsorption capacity of 177.66 mg/g. At acidic condition, excess H^+ ions induced AWAC's naturally negatively charged surface to be neutral, thus reducing the affinity of positively charged MB dye towards it. As the pH increased to 4 and 6, the reduced quantity of H^+ ions in the solution had weakened the neutralizing process between AWAC's surface and H^+ ions, thus adsorption capacity increased to 189.66 and 229.32 mg/g, respectively. At pH 8 and 10, existence of OH^- ions in the solution induced the AWAC's surface to be more negatively charged that it already was. Therefore, enhanced adsorption capacity of 256.41 and 279.33 mg/g was achieved at pH 8 and 10, respectively. At these alkaline conditions, the magnitude of zeta potential for AWAC was lower than -5.17 . At pH 12, a small increment in adsorption capacity of 280.71 proved that further increasing of pH would not have any effect on the zeta potential of AWAC anymore. This is because optimum effect of induced process had been achieved. Similar result was obtained by Do et al. (2021) where MB adsorption percentage had risen from 94.60% to 97.50% as the pH of solution increased from 4 to 11.

3.4. Adsorption isotherms

The non-linear plots of isotherm models are given in Fig. 11 and their corresponding parameters are tabulated in Table 6. To find the best isotherm that fit the adsorption data, correlation coefficient, R^2 and error percentage were judged. It was clear that adsorption of MB onto AWAC was best described by Langmuir isotherm ($R^2 = 0.9970$ and error = 0.41%). This signified that the monolayer coverage of MB dye molecules was formed on the homogenous surface of AWAC (Garcia et al., 2018). Freundlich and Temkin isotherms produced quite high R^2 values of 0.9968 and 0.9418, respectively whereas DR isotherm produced unsatisfactory R^2 value of 0.5323. Maximum adsorption capacity, Q_m generated by Langmuir and DR isotherms were 338.29 and 120.90 mg/g, respectively. Since the adsorption follows Langmuir, therefore Q_m value generated by Langmuir is more credible. Q_m value of AWAC can be considered as relatively high compared to oak seeds-based

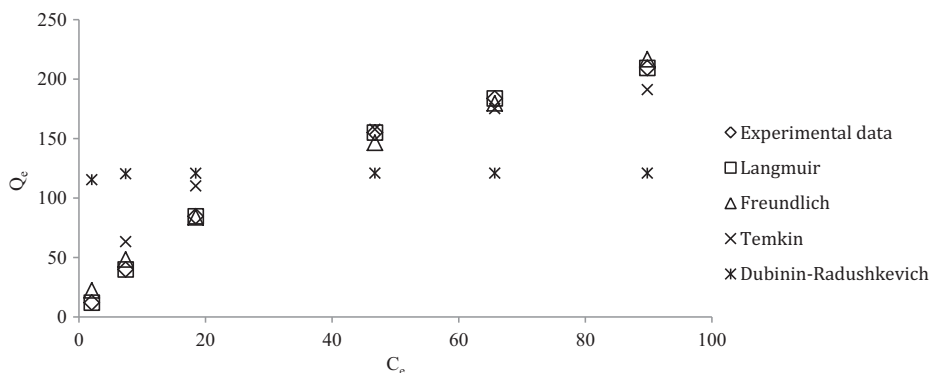


Fig. 11 Non-linear plots for isotherm models.

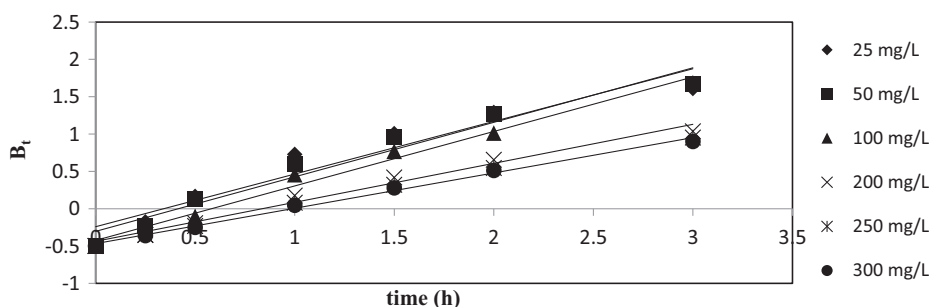


Fig. 12 Boyd plot.

Boyd plot was employed to further verify the actual slowest step in adsorption process (Garba and Rahim 2016). The Boyd plot is given in Fig. 12. Based on the Fig. 12, the lines for all initial concentrations of MB dye did not pass through the origin, thus confirming the rate limiting step in the adsorption process was film diffusion mechanism.

3.6. Adsorption thermodynamics

The values of ΔH° , ΔS° and E_a were determined to be -44.32 kJ/mol, -0.16 kJ/mol.K and 7.80 kJ/mol, respectively. Negative value obtained for ΔH° confirmed that the nature of adsorption process was exothermic where higher MB uptakes took place at lower solution temperature (Singh and Kuma, 2016). On the other hand, the negative value for ΔS° implied a decrease in randomness at the solid-liquid interface (Tharaneedhar et al., 2017). The adsorption of MB dye onto AWAC was controlled by physisorption since the E_a value is between 5 and 40 kJ/mol. Low activation energy values (< 42 kJ/mol) due to relatively weak temperature dependence of the pore diffusivity indicated diffusion-controlled process (Hao et al., 2020). Diffusion here refers to movement of solute to an external surface of adsorbent. Thus, the affinity of dyes onto activated carbon may be attributed to Van der Waals forces and electrostatic attractions between the dye and the surface of particles. Similar observation has been reported elsewhere (Basu et al., 2018; Aljeboree et al., 2015). Additionally, the values of ΔG° were found to be 2.74, 5.07 and 7.04 kJ/mol at temperature 303, 318 and 333 K, respectively. Moreover, the increase of ΔG° values with temperature signified that adsorption process was favoured at low temperature (Jung et al., 2017). Low ΔG° (< 20 kJ/mol) obtained in this investigation has also validated the physisorption nature of the adsorption process. The thermodynamics parameters obtained has succeeded in predicting how adsorption of dye might vary with temperature changes in adsorption system.

4. Conclusion

Acacia wood chip-based AC (AWAC) was successfully synthesized via microwave heating technique and physiochemical activation involving KOH chemical treatment and CO_2 gas treatment. The resulted AWAC was found to have high BET surface area of 1045.56 m²/g and mesopores surface area of 689.77 m²/g. RSM revealed the optimum preparation conditions of AWAC to be 360 W, 4.50 min and 0.90 g/g for radiation power, radiation time and IR, respectively. This

resulted in 81.20 mg/g of MB dye removal and 27.96% of AWAC yield. Based on F-value in ANOVA, radiation power and IR were found to affect the response of MB dye removal the most while radiation power and radiation time majorly impacted the response of AWAC's yield. Adsorption of MB dye onto AWAC was favoured at solution temperature of 30°C with adsorption capacity of 210.21 mg/g and at solution pH of 12 with MB removal of 280.71 mg/g. Isotherm and kinetic studies found that adsorption of MB onto AWAC follow Langmuir and PSO models, respectively. This is confirmed by Boyd plot which shows that the adsorption process was controlled by film diffusion mechanism and further affirmed by thermodynamic studies that revealed adsorption process was indeed exothermic, spontaneous, feasible and governed by physisorption.

Declaration of Competing Interest

The authors declare that they have no known competing financial interests or personal relationships that could have appeared to influence the work reported in this paper.

Acknowledgments

The authors thankfully acknowledge the financial support obtained from the Ministry of Higher Education (MOHE) via MyBrain15 scholarship and Universiti Sains Malaysia in terms of grant (Research University Grant: Number 8014061) and facilities.

Appendix A. Supplementary material

Supplementary data to this article can be found online at <https://doi.org/10.1016/j.arabjc.2021.103122>.

References

- Abbaszadeh, S., Wan Alwi, S.R., Webb, C., Ghasemi, N., Muhamad, I.I., 2016. Treatment of lead-contaminated water using activated carbon adsorbent from locally available papaya peel biowaste. *J. Cleaner Prod.* 118, 210–222. <https://doi.org/10.1016/j.jclepro.2016.01.054>.
- Ahmad, A.A., Din, A.T.M., Yahaya, N.K.E.M., Khasri, A., Ahmad, M.A., 2020. Adsorption of basic green 4 onto gasified Glyricidia sepium woodchip based activated carbon: Optimization, characterization, batch and column study. *Arabian J. Chem.* 13 (8), 6887–6903. <https://doi.org/10.1016/j.arabjc.2020.07.002>.

- Ahmad, M.A., Aswar, E.M., Oladoye, P.O., Adegok, K.A., Bell, O.S., 2021. Optimization and batch studies on adsorption of Methylene blue dye using pomegranate fruit peel based adsorbent. *Chem. Data Collect.* 100676. <https://doi.org/10.1016/j.cdc.2021.100676>.
- Aeenjan, F., Javanbakht, V., 2018. Methylene blue removal from aqueous solution by magnetic clinoptilolite/chitosan/EDTA nanocomposite. *Res. Chem. Intermed.* 44 (3), 1459–1483. <https://doi.org/10.1007/s11164-017-3179-x>.
- Agarwal, S., Gupta, V.K., Ghasemi, M., Azimi-Amin, J., 2017. Peganum harmala-L Seeds adsorbent for the rapid removal of noxious brilliant green dyes from aqueous phase. *J. Mol. Liq.* 231, 296–305. <https://doi.org/10.1016/j.molliq.2017.01.097>.
- Aljeboree, A.M., Alkaim, A.F., Al-Dujaili, A.H., 2015. Adsorption isotherm, kinetic modeling and thermodynamics of crystal violet dye on coconut husk-based activated carbon. *Desalin. Water Treat.* 53 (13), 3656–3667. <https://doi.org/10.1080/19443994.2013.877854>.
- Al-Ghouti, M.A., Al-Absi, R.S., 2020. Mechanistic understanding of the adsorption and thermodynamic aspects of cationic methylene blue dye onto cellulosic olive stones biomass from wastewater. *Sci. Rep.* 10 (1), 15928. <https://doi.org/10.1038/s41598-020-72996-3>.
- Amdoun, R., Khelifi, L., Khelifi-Slaoui, M., Amroune, S., Asch, M., Assaf-Ducrocq, C., Gontier, E., 2018. The desirability optimization methodology; a tool to predict two antagonist responses in biotechnological systems: case of biomass growth and hyoscyamine content in elicited datura starmonium hairy roots e1339 e1339 Iran. *J. Biotechnol.* 16 (1). <https://doi.org/10.21859/ijb.1339>.
- Arbanah, M., Miradatul, N.M., Ku, H.K., 2013. Utilization of pleurotus ostreatus in the removal of Cr (VI) from chemical laboratory waste. *Int. Refereed J. Eng. Sci.* 2, 29–39.
- Bashir, M.J.K., Aziz, H.A., Yusoff, M.S., Adlan, M.N., 2010. Application of response surface methodology (RSM) for optimization of ammoniacal nitrogen removal from semi-aerobic landfill leachate using ion exchange resin. *Desalination* 254, 154–161.
- Basu, S., Ghosh, G., Saha, S., 2018. Adsorption characteristics of phosphoric acid induced activation of bio-carbon: Equilibrium, kinetics, thermodynamics and batch adsorber design. *Process Saf. Environ. Protect.* 117, 125–142. <https://doi.org/10.1016/j.psep.2018.04.015>.
- Bedia, J., Peñas-Garzón, M., Gómez-Avilés, A., Rodríguez, J.J., Berver, C., 2020. Review on activated carbons by chemical activation with FeCl₃. *J. Carbon Res.* 6 (2), 21.
- Beltrame, K.K., Cazetta, A.L., de Souza, P.S.C., Spessato, L., Silva, T. L., Almeida, V.C., 2018. Adsorption of caffeine on mesoporous activated carbon fibers prepared from pineapple plant leaves. *Ecotoxicol. Environ. Saf.* 147, 64–71. <https://doi.org/10.1016/j.ecoenv.2017.08.034>.
- Boopathy, R., Karthikeyan, S., Mandal, A.B., Sekaran, G., 2013. Adsorption of ammonium ion by coconut shell-activated carbon from aqueous solution: kinetic, isotherm, and thermodynamic studies. *Environ. Sci. Pollut. Res.* 20 (1), 533–542. <https://doi.org/10.1007/s11356-012-0911-3>.
- Borghei, S.A., Zare, M.H., Ahmadi, M., Sadeghi, M.H., Marjani, A., Shirazian, S., Ghadiri, M., 2021. Synthesis of multi-application activated carbon from oak seeds by KOH activation for methylene blue adsorption and electrochemical supercapacitor electrode. *Arabian J. Chem.* 14 (2), 102958. <https://doi.org/10.1016/j.arabjc.2020.102958>.
- Chen, W., He, F., Zhang, S., Xv, H., Xv, Z., 2018. Development of porosity and surface chemistry of textile waste jute-based activated carbon by physical activation. *Environ. Sci. Pollut. Res.* 25 (10), 9840–9848. <https://doi.org/10.1007/s11356-018-1335-5>.
- Dai, Y., Zhang, N., Xing, C., Cui, Q., Sun, Q., 2019. The adsorption, regeneration and engineering applications of biochar for removal organic pollutants: A review. *Chemosphere* 223, 12–27. <https://doi.org/10.1016/j.chemosphere.2019.01.161>.
- Danish, M., Ahmad, T., Hashim, R., Said, N., Akhtar, M.N., Mohamad-Saleh, J., Sulaiman, O., 2018. Comparison of surface properties of wood biomass activated carbons and their application against rhodamine B and methylene blue dye. *Surf. Interfaces* 11, 1–13. <https://doi.org/10.1016/j.surfin.2018.02.001>.
- Danish, M., Birnbach, J., Mohamad Ibrahim, M.N., Hashim, R., 2020. Scavenging of caffeine from aqueous medium through optimized H₃PO₄-activated Acacia mangium wood activated carbon: Statistical data of optimization. *Data Brief* 28, <https://doi.org/10.1016/j.dib.2019.105045> 105045.
- Danish, M., Hashim, R., Ibrahim, M.N.M., Rafatullah, M., Sulaiman, O., 2012. Surface characterization and comparative adsorption properties of Cr(VI) on pyrolysed adsorbents of Acacia mangium wood and Phoenix dactylifera L. stone carbon. *J. Anal. Appl. Pyrol.* 97, 19–28. <https://doi.org/10.1016/j.jaap.2012.06.001>.
- Daoud, M., Benturki, O., Kecira, Z., Girods, P., Donnot, A., 2017. Removal of reactive dye (BEZAKTIV Red S-MAX) from aqueous solution by adsorption onto activated carbons prepared from date palm rachis and jujube stones. *J. Mol. Liq.* 243, 799–809. <https://doi.org/10.1016/j.molliq.2017.08.093>.
- Das, A., Mishra, S., 2017. Removal of textile dye reactive green-19 using bacterial consortium: Process optimization using response surface methodology and kinetics study. *J. Environ. Chem. Eng.* 5 (1), 612–627. <https://doi.org/10.1016/j.jece.2016.10.005>.
- Do, T.H., Nguyen, V.T., Dung, N.Q., Chu, M.N., Van Kiet, D., Ngan, T.T.K., Van Tan, L., 2021. Study on methylene blue adsorption of activated carbon made from Moringa oleifera leaf. *Mater. Today: Proc.* <https://doi.org/10.1016/j.matpr.2020.10.834>.
- Doumic, L., Salierno, G., Cassanello, M., Haure, P., Ayude, M., 2015. Efficient removal of Orange G using Prussian Blue nanoparticles supported over alumina. *Catal. Today* 240, 67–72. <https://doi.org/10.1016/j.cattod.2014.03.064>.
- Foo, K., Hameed, B., 2012. Preparation, characterization and evaluation of adsorptive properties of orange peel based activated carbon via microwave induced K₂CO₃ activation. *Bioresour. Technol.* 104, 679–686.
- Freundlich, H.M.F., 1906. Over the adsorption in solution. *J. Phys. Chem.* 57, 385–471.
- Garba, Z.N., Rahim, A.A., 2016. Evaluation of optimal activated carbon from an agricultural waste for the removal of para-chlorophenol and 2,4-dichlorophenol. *Process Saf. Environ. Prot.* 102, 54–63. <https://doi.org/10.1016/j.psep.2016.02.006>.
- Garcia, J.R., Sedran, U., Zaini, M.A.A., Zakaria, Z.A., 2018. Preparation, characterization and dye removal study of activated carbon prepared from palm kernel shell. *Environ. Sci. Pollut. Res.* 25, 5076–5085.
- Ghaedi, M., Khafri, H.Z., Asfaram, A., Goudarzi, A., 2016. Response surface methodology approach for optimization of adsorption of Janus Green B from aqueous solution onto ZnO/Zn(OH)₂-NP-AC: kinetic and isotherm study. *Spectrochim. Acta, Part A Mol. Biomol. Spectrosc.* 152, 233–240.
- Ghaedi, M., Nasab, A., Khodadoust, S., Sahraei, R., Daneshfar, A., 2015. Characterization of zinc oxide nanorods loaded on activated carbon as cheap and efficient adsorbent for removal of methylene blue. *J. Ind. Eng. Chem.* 21, 986–993.
- Ghani, Z.A., Yusoff, M.S., Zaman, N.Q., Zamri, M.F.M.A., Andas, J., 2017. Optimization of preparation conditions for activated carbon from banana pseudo-stem using response surface methodology on removal of color and COD from landfill leachate. *Waste Manage.* 62, 177–187.
- González-García, P., 2018. Activated carbon from lignocellulosics precursors: A review of the synthesis methods, characterization techniques and applications. *Renew. Sustain. Energy Rev.* 82, 1393–1414. <https://doi.org/10.1016/j.rser.2017.04.117>.
- Guclu, C., Alper, K., Erdem, M., Tekin, K., Karagoz, S., 2021. Activated carbons from co-carbonization of waste truck tires and spent tea leaves. *Sustainable Chem. Pharm.* 21, <https://doi.org/10.1016/j.scp.2021.100410> 100410.
- Hao, L., Gao, W., Yan, S., Niu, M., Liu, G., Hao, H., 2020. Functionalized diatomite/oyster shell powder doped electrospun polyacrylonitrile submicron fiber as a high-efficiency adsorbent for

- removing methylene blue from aqueous solution: Thermodynamics, kinetics and isotherms. *J. Mol. Liq.* 298, <https://doi.org/10.1016/j.molliq.2019.112022> 112022.
- Ho, Y.S., McKay, G., 1999. Pseudo-second order model for sorption processes. *Process Biochem.* 34 (5), 451–465. [https://doi.org/10.1016/S0032-9592\(98\)00112-5](https://doi.org/10.1016/S0032-9592(98)00112-5).
- Ilnicka, A., Kamedulski, P., Aly, H.M., Lukaszewicz, J.P., 2020. Manufacture of activated carbons using Egyptian wood resources and its application in oligothiophene dye adsorption. *Arabian J. Chem.* 13 (5), 5284–5291. <https://doi.org/10.1016/j.arabjc.2020.03.007>.
- Islam, M.A., Benhouria, A., Asif, M., Hameed, B., 2015. Methylene blue adsorption on factory-rejected tea activated carbon prepared by conjunction of hydrothermal carbonization and sodium hydroxide activation processes. *J. Taiwan Inst. Chem. Eng.* 52, 57–64.
- Islam, M.A., Sabar, S., Benhouria, A., Khanday, W.A., Asif, M., Hameed, B.H., 2017. Nanoporous activated carbon prepared from karanj (*Pongamia pinnata*) fruit hulls for methylene blue adsorption. *J. Taiwan Inst. Chem. Eng.* 74, 96–104. <https://doi.org/10.1016/j.jtice.2017.01.016>.
- Izgi, M.S., Saka, C., Baytar, O., Saraçoğlu, G., Şahin, Ö., 2019. Preparation and characterization of activated carbon from microwave and conventional heated almond shells using phosphoric acid activation. *Anal. Lett.* 52 (5), 772–789. <https://doi.org/10.1080/00032719.2018.1495223>.
- Jang, H.M., Kan, E., 2019. A novel hay-derived biochar for removal of tetracyclines in water. *Bioresour. Technol.* 274, 162–172. <https://doi.org/10.1016/j.biortech.2018.11.081>.
- Jia, P., Tan, H., Liu, K., Gao, W., 2018. Removal of methylene blue from aqueous solution by bone char. *Appl. Sci.* 8 (10), 1903.
- Jung, K.-W., Choi, B.H., Hwang, M.-J., Choi, J.-W., Lee, S.-H., Chang, J.-S., Ahn, K.-H., 2017. Adsorptive removal of anionic azo dye from aqueous solution using activated carbon derived from extracted coffee residues. *J. Cleaner Prod.* 166, 360–368. <https://doi.org/10.1016/j.jclepro.2017.08.045>.
- Kacan, E., 2016. Optimum BET surface areas for activated carbon produced from textile sewage sludges and its application as dye removal. *J. Environ. Manage.* 166, 116–123. <https://doi.org/10.1016/j.jenvman.2015.09.044>.
- Khanday, W.A., Asif, M., Hameed, B.H., 2017a. Cross-linked beads of activated oil palm ash zeolite/chitosan composite as a bio-adsorbent for the removal of methylene blue and acid blue 29 dyes. *Int. J. Biol. Macromol.* 95, 895–902. <https://doi.org/10.1016/j.ijbiomac.2016.10.075>.
- Khanday, W.A., Marrakchi, F., Asif, M., Hameed, B.H., 2017b. Mesoporous zeolite-activated carbon composite from oil palm ash as an effective adsorbent for methylene blue. *J. Taiwan Inst. Chem. Eng.* 70, 32–41. <https://doi.org/10.1016/j.jtice.2016.10.029>.
- Khasri, A., Bello, O.S., Ahmad, M.A., 2018. Mesoporous activated carbon from Pentace species sawdust via microwave-induced KOH activation: optimization and methylene blue adsorption. *Res. Chem. Intermed.* 44 (10), 5737–5757. <https://doi.org/10.1007/s11164-018-3452-7>.
- Kono, H., 2015. Preparation and characterization of amphoteric cellulose hydrogels as adsorbents for the anionic dyes in aqueous solutions. *Gels* 1, 94–116.
- Kumar, A., Jena, H.M., 2016. Preparation and characterization of high surface area activated carbon from Fox nut (*Euryale ferox*) shell by chemical activation with H₃PO₄. *Results Phys.* 6, 651–658. <https://doi.org/10.1016/j.rinp.2016.09.012>.
- Kushwaha, A.K., Gupta, N., Chattopadhyaya, M.C., 2014. Removal of cationic methylene blue and malachite green dyes from aqueous solution by waste materials of *Daucus carota*. *J. Saudi Chem. Soc.* 18, 200–207.
- Lagergren, S., Svenska, K., 1898. About the theory of so-called adsorption of soluble substances. 24, 1–39.
- Lam, S.S., Wan Mahari, W.A., Cheng, C.K., Omar, R., Chong, C.T., Chase, H.A., 2016. Recovery of diesel-like fuel from waste palm oil by pyrolysis using a microwave heated bed of activated carbon. *Energy* 115, 791–799. <https://doi.org/10.1016/j.energy.2016.09.076>.
- Langmuir, I., 1918. The adsorption of gases on plane surfaces of glass, mica and platinum. *J. Am. Chem. Soc.* 40 (9), 1361–1403.
- Li, Y., Liu, Y., Yang, W., Liu, L., Pan, J., 2021. Adsorption of elemental mercury in flue gas using biomass porous carbons modified by microwave/hydrogen peroxide. *Fuel* 291, <https://doi.org/10.1016/j.fuel.2021.120152> 120152.
- Liew, R.K., Azwar, E., Yek, P.N.Y., Lim, X.Y., Cheng, C.K., Ng, J.-H., Lam, S.S., 2018. Microwave pyrolysis with KOH/NaOH mixture activation: A new approach to produce micro-mesoporous activated carbon for textile dye adsorption. *Bioresour. Technol.* 266, 1–10. <https://doi.org/10.1016/j.biortech.2018.06.051>.
- Lima, E.C., Hosseini-Bandegharaei, A., Moreno-Piraján, J.C., Anastopoulos, I., 2019. A critical review of the estimation of the thermodynamic parameters on adsorption equilibria. Wrong use of equilibrium constant in the Van't Hoff equation for calculation of thermodynamic parameters of adsorption. *J. Mol. Liq.* 273, 425–434. <https://doi.org/10.1016/j.molliq.2018.10.048>.
- Lopes, G.K.P., Zanella, H.G., Spessato, L., Ronix, A., Viero, P., Fonseca, J.M., Almeida, V.C., 2021. Steam-activated carbon from malt bagasse: Optimization of preparation conditions and adsorption studies of sunset yellow food dye. *Arabian J. Chem.* 14, (3). <https://doi.org/10.1016/j.arabjc.2021.103001> 103001.
- Mahapatra, U., Chatterjee, A., Das, C., Manna, A.K., 2021. Adsorptive removal of hexavalent chromium and methylene blue from simulated solution by activated carbon synthesized from natural rubber industry biosludge. *Environ. Technol. Innovation* 101427. <https://doi.org/10.1016/j.eti.2021.101427>.
- Marrakchi, F., Ahmed, M.J., Khanday, W.A., Asif, M., Hameed, B. H., 2017. Mesoporous-activated carbon prepared from chitosan flakes via single-step sodium hydroxide activation for the adsorption of methylene blue. *Int. J. Biol. Macromol.* 98, 233–239. <https://doi.org/10.1016/j.ijbiomac.2017.01.119>.
- Marrakchi, F., Khanday, W.A., Asif, M., Hameed, B.H., 2016. Cross-linked chitosan/sepiolite composite for the adsorption of methylene blue and reactive orange 16. *Int. J. Biol. Macromol.* 93 (Pt A), 1231–1239. <https://doi.org/10.1016/j.ijbiomac.2016.09.069>.
- Maršálek, R., Švidrnoch, M., 2020. The adsorption of amitriptyline and nortriptyline on activated carbon, diosmectite and titanium dioxide. *Environ. Challenges* 1. <https://doi.org/10.1016/j.envc.2020.100005> 100005.
- Medhat, A., El-Maghrabi, H.H., Abdelghany, A., Abdel Menem, N. M., Raynaud, P., Moustafa, Y.M., et al., 2021. Efficiently activated carbons from corn cob for methylene blue adsorption. *Applied Surface Science Advances* 3. <https://doi.org/10.1016/j.ap-sadv.2020.100037> 100037.
- Melliti, A., Srivastava, V., Kheriji, J., Sillanpää, M., Hamrouni, B., 2021. Date Palm Fiber as a novel precursor for porous activated carbon: Optimization, characterization and its application as Tylosin antibiotic scavenger from aqueous solution. *Surf. Interfaces* 101047. <https://doi.org/10.1016/j.surfin.2021.101047>.
- Njoku, V.O., Foo, K.Y., Asif, M., Hameed, B.H., 2014. Preparation of activated carbons from rambutan (*Nephelium lappaceum*) peel by microwave-induced KOH activation for acid yellow 17 dye adsorption. *Chem. Eng. J.* 250, 198–204. <https://doi.org/10.1016/j.cej.2014.03.115>.
- Porhemmat, S., Ghaedi, M., Rezvani, A.R., Azghandi, M.H.A., Bazrafshan, A.A., 2017. Nanocomposites: Synthesis, characterization and its application to removal azo dyes using ultrasonic assisted method: Modeling and optimization. *Ultrasonics Sonochemistry* 38, 530–543. <https://doi.org/10.1016/j.ultsonch.2017.03.053>.
- Rashidi, N.A., Yusop, S., 2017. A review on recent technological advancement in the activated carbon production from oil palm wastes. *Chem. Eng. J.* 314, 277–290. <https://doi.org/10.1016/j.cej.2016.11.059>.

- Redlich, O., Peterson, D.L., 1959. A useful adsorption isotherm 1024 1024 *J. Phys. Chem.* 63 (6). <https://doi.org/10.1021/j150576a611>.
- Singh, V.K., Kuma, E.A., 2016. Measurement and analysis of adsorption isotherms of CO₂ on activated carbon. *Appl. Therm. Eng.* 97, 77–86.
- Sousa, É., Rocha, L., Jaria, G., Gil, M.V., Otero, M., Esteves, V.I., Calisto, V., 2021. Optimizing microwave-assisted production of waste-based activated carbons for the removal of antibiotics from water. *Sci. Total Environ.* 752,. <https://doi.org/10.1016/j.scitotenv.2020.141662> 141662.
- Temkin, M.I., Pyzhev, V., 1940. Kinetics and ammonia synthesis on promoted iron catalyst. *Acta Physiochim. USSR* 12, 327–356.
- Tharaneedhar, V., Senthil Kumar, P., Saravanan, A., Ravikumar, C., Jaikumar, V., 2017. Prediction and interpretation of adsorption parameters for the sequestration of methylene blue dye from aqueous solution using microwave assisted corncob activated carbon. *Sustainable Mater. Technol.* 11, 1–11. <https://doi.org/10.1016/j.susmat.2016.11.001>.
- Tounsadi, H., Khalidi, A., Farnane, M., Abdennouri, M., Barka, N., 2016. Experimental design for the optimization of preparation conditions of highly efficient activated carbon from *Glebionis coronaria* L. and heavy metals removal ability. *Process Saf. Environ. Prot.* 102, 710–723. <https://doi.org/10.1016/j.psep.2016.05.017>.
- Wan Mahari, W.A., Zainuddin, N.F., Wan Nik, W.M.N., Chong, C. T., Lam, S.S., 2016. Pyrolysis recovery of waste shipping oil using microwave heating. *Energies* 9 (10), 780.
- Yağmur, H.K., Kaya, İ., 2021. Synthesis and characterization of magnetic ZnCl₂-activated carbon produced from coconut shell for the adsorption of methylene blue. *J. Mol. Struct.* 1232,. <https://doi.org/10.1016/j.molstruc.2021.130071> 130071.
- Yorgun, S., Yildiz, D., 2015. Preparation and characterization of activated carbons from Paulownia wood by chemical activation with H₃PO₄. *J. Taiwan Inst. Chem. Eng.* 53, 122–131.
- Yusop, M.F.M., Ahmad, M.A., Rosli, N.A., Gonawan, F.N., Abdullah, S.J., 2021. Scavenging malachite green dye from aqueous solution using durian peel based activated carbon. *Malaysian J. Fundam. Appl. Sci.* 17 (1), 95–103.
- Zhang, X., Duan, C., Jia, X., Dai, B., 2016. Carboxylation kapok fiber as a low-cost, environmentally friendly adsorbent with remarkably enhanced adsorption capacity for cationic dyes. *Res. Chem. Intermed.* 42, 5069–5085.
- Zhang, Z., Xu, L., Liu, Y., Feng, R., Zou, T., Zhang, Y., Zhou, P., 2021. Efficient removal of methylene blue using the mesoporous activated carbon obtained from mangosteen peel wastes: Kinetic, equilibrium, and thermodynamic studies. *Microporous Mesoporous Mater.* 315,. <https://doi.org/10.1016/j.micromeso.2021.110904> 110904.
- Zhou, L., Yu, Q., Cui, Y., Xie, F., Li, W., Li, Y., Chen, M., 2017. Adsorption properties of activated carbon from reed with a high adsorption capacity. *Ecol. Eng.* 102, 443–450. <https://doi.org/10.1016/j.ecoleng.2017.02.036>.
- Zhou, D., Li, D., Li, A., Qi, M., Cui, D., Wang, H., Wei, H., 2021. Activated carbons prepared via reflux-microwave-assisted activation approach with high adsorption capability for methylene blue. *J. Environ. Chem. Eng.* 9, (1). <https://doi.org/10.1016/j.jece.2020.104671> 104671.